Shift current in the ferroelectric semiconductor SbSI

N. Ogawa, M. Sotome, Y. Kaneko, M. Ogino, and Y. Tokura

Phys. Rev. B **96**, 241203 — Published 26 December 2017

DOI: 10.1103/PhysRevB.96.241203

Shift current in ferroelectric semiconductor SbSI

N. Ogawa,[1,2] M. Sotome,[1] Y. Kaneko,[1] M. Ogino,[3] and Y. Tokura[1,4]

[1]*RIKEN Center for Emergent Matter Science (CEMS), Wako, Saitama 351-0198, Japan*

[2]*PRESTO, Japan Science and Technology Agency (JST), Kawaguchi 332-0012**

[3]*Department of Applied Physics, University of Tokyo, Tokyo 113-8656, Japan*

[4]*Department of Applied Physics and Quantum-Phase Electronics Center (QPEC), University of Tokyo, Tokyo 113-8656, Japan*

(Dated: December 7, 2017)

Abstract

Spontaneous photocurrent, termed shift current, can flow in noncentrosymmetric bulk crystals due to topological nature of constituting electronic bands. The shift current with less-dissipative character may have remarkable advantages over the conventional drift photocurrent driven by built-in potential or external electric field. We revisit the generation and transport of shift current in a prototypical ferroelectric semiconductor SbSI near its band gap energy. It is revealed that the switchable shift current is steadily generated by photoexcitation down to low temperature, appears over a distance of millimeter range in a highly insulating bulk without noticeable decay, and largely exceeds polarization charge in the sample, reflecting its Berry phase origin.

PACS numbers: 72.40.+w, 77.80.-e, 78.47.jh, 03.65.Vf

There has been a renewed interest in the shift current, one of the bulk photovoltaic phenomena in noncentrosymmetric media with above-band-gap excitation, especially after the discovery of its Berry phase contributions. Following consecutive theoretical and experimental efforts[1–5], it is nowadays possible to predict the shift current spectra from first-principles calculations[6]. In contrast to the conventional drift photocurrent under the electric field, the photoexcited carriers coherently shift in real space due to the difference in the Berry connection between valence and conduction bands. The transport of shift current is in principle related to the coherence of wave functions[7], having a potential to realize less-dissipative energy flow.

The optimal efficiency for the generation of shift current has been intensively discussed recently[8–11]. The shift mechanism is advantageous because (i) whole sample volume contributes to the photocurrent generation, (ii) it is responsive to unpolarized light, and (iii) open-circuit voltage (V_{OC}) can largely exceed the band gap energy. Generally, low-dimensional materials with large density-of-states near the band edge are desirable for the photocurrent generation. In addition, highly insulating bulk is helpful to yield larger V_{OC} and to avoid carrier scatterings. In reality, however, the situation is highly dependent on the characters of contributing electronic bands.

In this *Communication*, we revisit the zero-bias photocurrent in a prototypical ferroelectric semiconductor to unveil nonequilibrium electron transport by the shift current. We select the sample, antimony sulfuriodide (SbSI), with the band gap in visible wavelength and the ferroelectric transition near room temperature, and focus on the carrier dynamics excited locally by pulsed lasers. We found that the photocurrent can be excited at any location in the sample down to low temperature, appears at the electrodes through a highly insulating bulk without noticeable decay, largely exceeds the polarization charge (stored by spontaneous polarization, Ps) when accumulated in time, and is intact from other photoeffects. These characteristics experimentally confirm the appearance of the shift current, originating from the topology of electronic bands.

SbSI is a semiconductor with an indirect and direct band gap of $\sim$1.8 eV and $\sim$2.0 eV, respectively[12]. SbSI is composed of double chain-like ensemble [Fig. 1(a)][13], and shows ferroelectric transition upon cooling at Curie temperature $T_{\rm C}\sim$295 K with the Ps amplitude of $\sim$25 μC/cm^2 along the c-axis, while changing the point group from D_{2h} to C_{2v} (Ref. 14). After the discovery of its ferroelectricity[15], extensive efforts have been devoted to uncover

its photo-induced properties, i.e., photoferroelectric effects including changes in the Ps, T_C, band gap, charging of trap states, photostriction, photorefractive properties, etc.[16,17], which are followed by recent interests for solar cell applications[18–21]. In these ferroelectric semiconductors, V_{OC} can exceed 10^3 V upon photoexcitation[17]. It is noted that SbSI can have a Rashba-type spin splitting to show circular photogalvanic effects[22], whose sign can be reversed by the orientation of Ps[23].

Single crystals of SbSI were grown by a chemical vapor transport technique. Several samples with square pole shape were selected and illuminated by various light sources, including a monochromated halogen lamp, continuous-wave (cw) laser diodes (LD), and a wavelength-tunable pulsed laser (120 fs, 1 kHz). Two-terminal electrodes were prepared by depositing AuPd or directly by Ag paste. The observed optical characteristics are reproducible, and in the following we show the data from a relatively long single-crystal with the dimension of 0.45 x 0.45 x 4.8 mm^3 (c along the longest axis). The photocurrent was detected by a commercial source-measure unit (SMU) or by using a wide-band preamplifier (band-width of 200 MHz). All samples are highly insulating and show the similar physical properties with some variations in the photocurrent amplitude, due probably to the habit of each crystal and Schottky-like barriers formed near the electrodes. Prior to the photocurrent measurements, these samples were poled by cooling under the external electric field (indicated as $\pm P$ poling, hereafter) from $\sim$320 K. The point symmetry of the sample was also checked by optical second harmonic generation (SHG) with 1.55 eV fundamental light.

Figure 1 shows the basic ferroelectric and photocurrent characteristics of a SbSI single crystal. The T_C and Ps amplitude, as measured by integrating the pyroelectric current [Fig. 1(b)], are found to be consistent with previous reports[15]. With illumination by cw light sources, the drift photocurrent flows following the external bias voltage, whereas the zero-bias photocurrent appears in the opposite direction, both with the maximum efficiency around the band gap [Fig. 1(c)][24,25]. The zero-bias photocurrent shows a peak around 260 K in the temperature scan [Fig. 1(d)]. Figures 1(e) and 1(f) show I-V characteristics for $\pm P$ poling, respectively, under illumination, illustrating the poling-dependent zero-bias photocurrent and near-linear transport properties at this temperature. The V_{OC} rapidly grows toward low temperature (not shown) in accord with the sample resistance, as observed in many photovoltaic ferroelectrics[17]. We adopt $E(\omega)//c$ excitation, i.e., the light polarization is parallel to the spontaneous polarization Ps, in the following.

SbSI is known to have many defect levels, which make a tail of the photocurrent spectrum in the band gap [Fig. 1(c)][26]. Therefore a care should be taken when evaluating its photoeffects. Figure 2 illustrates the time-trace of the photocurrent. For cw illumination (at 1.95 eV), the zero-bias photocurrent shows a transient with a decay time of ∼30 seconds, followed by a slow relaxation lasting over 400 minutes [Fig. 2(a)]. Thus the data in Fig. 1 are inevitably taken in this transient/relaxation regime. In contrast, with pulsed excitation (at 2.05 eV) the zero-bias photocurrent indicates no characteristic relaxation as shown in Fig. 2(b). In both cases, the integrated charges largely exceed the Ps (stored charge by poling), confirming that the observed zero-bias current is not from pyroelectric discharge, but from an anomalous photovoltaic effect in ferroelectric media. Note that the penetration depth is evaluated to be 9 μm and 4 μm at 1.95 eV and 2.05 eV, respectively. The difference between cw and pulse excitation appears due to several reasons; for the cw case, some of the carriers will be trapped by defect levels, and also accumulate near the electrodes with Schottky-like barriers, which leads to a modification in the potential distribution inhibiting further charge transport. In contrast, pulsed photocurrent can go through these barriers by capacitive coupling, i.e., the capacitors formed at the electrodes are transparent to the pulsed current. The efficiency of photocurrent generation is evaluated to be 10^{-6}-10^{-7} electron/photon. However, actual efficiency for the pulsed excitation should be much better, considering the ultrafast nature of the shift current[27,28] and limited bandwidth in cables (∼5 GHz) or in the preamplifier (200 MHz).

Next we characterize the photocarrier transport by scanning the excitation spot [Fig. 3(a)]. With an external bias voltage, the drift photocurrent is found to be larger at the location close to the electrode with positive bias. This distribution is reversed by switching the bias polarity [Fig. 3(b)]. The zero-bias photocurrent also appears all along the sample crystal, with somewhat sample-dependent current distributions [Fig. 3(c)]. The similar nonlocal transports of shift current have been reported recently[7,29]. It is seen that, with the same poling condition, the cw and pulsed laser excitation show a qualitatively similar photocurrent distribution, indicating the same physical origin. Figure 3(d) depicts the time-traces of the pulsed photocurrent measured at three locations on the sample. There is no apparent time-delay in the arrival of photocurrent pulse in the preamplifier within our experimental resolution (∼2 ns).

One might think that the zero-bias photocurrent in Fig 3(c) is just a drift photocurrent

driven by uncompensated internal electric fields. However, in that case, the photocurrent would decrease much faster at the location away from the positive electrode, similarly to that in Fig. 3(b). The asymmetric spatial distribution in the zero-bias photocurrent can be ascribed to the possible habit of individual sample crystals, as reported previously[30].

It is also found that the photo-Hall effect, transverse photocurrent as a function of applied magnetic field, is absent in our samples (Fig 3(e)). For this measurement, two additional electrodes were attached near the center of the sample, and an external magnetic field was applied normal to the surface. The incident laser was linearly-polarized along the c-axis and focused between the electrodes, for which the photocurrent is expected to appear only along the c-axis due to the C_{2v} symmetry. The small but finite Hall-current, independent of the external magnetic field, can be ascribed to the slight asymmetry in these transverse electrodes. The absence of the photo-Hall effect and the prefect reversal of photocurrent upon opposite poling support that the ballistic photocurrent[17,31] is not relevant in our observation. Note that the spatial-oscillation of the photocurrent due to the optical birefringence[2], which may cancel the photo-Hall current, can be ruled out, since we illuminate the sample along one of the crystallographic axes and with the light polarization exactly along the c-axis ($E(\omega)//c$).

The photon energy and temperature dependence of the zero-bias photocurrent under pulsed excitation are shown in Fig. 4. We found an anomaly, that is a transient and opposite (positive) current flow, with the incident photon energy near the band edge [Fig. 4(a)]. This current component is present in the limited temperature range, just below the $T_{\rm C}$ [Fig. 4(b)]. It is interesting that if we integrate the photocurrent in the time-trace, this anomaly becomes mostly invisible [Fig. 4(c)]. The nearly constant charge yield down to low temperature as observed in this figure, which is distinct from that of the cw excitation shown in Fig. 1(d), supports our understanding that the shift current is insensitive to the sample resistivity and barrier formation near the electrodes. Thus the intrinsic shift current properties can be revealed by using pulsed optical excitation. The shift current is also insensitive to external bias voltage[9] as exemplified in Fig. 4(d). Note that the relaxation profiles of photocurrent in Fig. 4 are influenced by the transient sample capacitance as well as by the bandwidth of the preamplifier.

Now we discuss the partially reversed photocurrent in the time-trace in Figs. 4(a) and 4(b). The photocurrent peak observed in the temperature dependence under the cw excitation [Fig. 1(d)] indicates a finite contribution of thermo- and photo-stimulated carrier

emission from trap states[17], which would also appear in the pulsed photocurrent. However, if these carriers were driven by the internal electric field, their response would be much slower. Moreover, the cw and pulsed laser excitation would show nearly the same temperature dependence, which is not the case here [compare Fig. 1(d) and Fig. 4(c)]. In reality, a similar anomaly in the photon energy dependence can be found in the photostriction of SbSI, where the coefficient of strain changes its sign just around the band gap[25]. This sign reversal has been discussed to be due to the competition among the photoinduced change in the Ps, screening by the photocarrier, and modification of domain structures[27,32]. The latter, macroscopic rearrangement of domains would, however, be much slower than the time-scale of pulsed photocurrent. The temperature-independent charge yield [Fig. 4(c)] implies the absence of additional photocurrent sources, such as shift current from other bands or from defect states. Therefore we propose that the fast and reversed photocurrent appears in Fig. 4 due to the transient change in the Ps, which recovers subsequently and does not contribute to the total charge detected through the electrodes. This change in local Ps (or dielectric constant) affects the electrode charges in an ultrafast manner, supposing that the sample and electrodes form a big capacitor. We can safely exclude the possibility of local (and persistent) depolarization because of the steady photocurrent generation observed in Fig. 2(b).

The above observations indicate that intrinsic characters of shift photocurrent can be unveiled by comparing the carrier dynamics under cw and pulsed excitation. It is revealed that the shift current appears at any location in the single crystal, appears at the electrodes over a distance of millimeter range in a highly insulating bulk without noticeable decay, and persists down to low temperature for the case of pulsed excitation. The accumulated shift current largely exceeds the polarization charge, and is not affected by other photoeffects. The fast, dissipation-less, and long-range propagation of shift current points to the novel aspects of the shift current coming from its topological origin, thus providing an important arena of the photonic functions to be explored in materials with broken inversion symmetry.

ACKNOWLEDGMENTS

The authors thank T. Morimoto, W. Koshibae, M. Nakamura, M. Kawasaki, and N. Nagaosa for stimulating discussions. This research is supported by CREST and PRESTO

JST, and also by the JSPS KAKENHI No. 24224009, No. 16K13705, and No. 17H02914.

---

* naoki.ogawa@riken.jp

[1] R. von Baltz and W. Kraut, Phys. Rev. B **23,** 5590 (1981).

[2] B. I. Sturman and V. M Fridkin, *The Photovoltaic and Photorefractive Effects in Noncentrosymmetric Materials* (Breach Science Publishers, 1992).

[3] J. E. Sipe and A. I. Shkrebtii, Phys. Rev. B **61,** 5337 (2000).

[4] F. Nastos and J. E. Sipe, Phys. Rev. B **82,** 235204 (2010).

[5] T. Morimoto and N. Nagaosa, Sci. Adv. **2,** e1501524 (2016).

[6] S. M. Young and A. M. Rappe, Phys. Rev. Lett. **109,** 116601 (2012).

[7] H. Ishizuka and N. Nagaosa, New J. Phys. **19,** 033015 (2017).

[8] I. Grinberg, D. V. West, M. Torres, G. Gou, D M. Stein, L. Wu, G. Chen, E. M. Gallo, A. R. Akbashev, P. K. Davies, J. E. Spanier, and A. M. Rappe Nature **503,** 509 (2013).

[9] L. Z. Tan, F. Zheng, S. M. Young, F. Wang, S. Liu, and A. M. Rappe, npj Comp. Mater. **2,** 16026 (2016).

[10] W. Ji, K. Yao, and Y. C. Liang, Adv. Mater. **22,** 1763 (2016).

[11] A. M. Cook, B. M. Fregoso, F. de Juan, S. Coh, and J. E. Moore, Nature Commun. **8,** 14176 (2017).

[12] M. Nowak, B. Kauch, and P. Szperlich, Rev. Sci. Instrum. **80,** 046107 (2009).

[13] K. Momma and F. Izumi, J. Appl. Crystallogr. **44,** 1272 (2011).

[14] A. Kikuchi, Y. Oka, and E. Sawaguchi, J. Phys. Soc. Jpn. **23,** 337 (1967).

[15] E. Fatuzzo, G. Harbeke, W. J. Merz, R. Nitsche, H. Roetschi, and N. Ruppel, Phys. Rev. **127,** 2036 (1962).

[16] R. Nietsche and W. J. Mertz, J. Phys. Chem. Solids **13,** 154 (1960).

[17] V. M. Fridkin, *Photoferroelectrics* (Springer-Verlag, New York 1979), and references therein.

[18] H. Akkus and A. M. Mamedov, CEJP **5,** 25 (2007).

[19] M. Nowak, Ł. Bober, B. Borkowski, M. Kępińska, P. Szperlich, D. Stróż, and M. Sozańska, Opt. Mater. **35,** 2208 (2007).

[20] K. T. Butler, J. M. Frost, and A. Walsh, Energy Environ. Sci. **8,** 838 (2015).

[21] K. T. Butler, S. McKechnie, P. Azarhoosh, M. van Schilfgaarde, D. O. Scanlon, and A. Walsh,

Appl. Phys. Lett. **108,** 112103 (2016).

[22] N. Ogawa, M. S. Bahramy, Y. Kaneko, and Y. Tokura, Phys. Rev. B **90,** 125122 (2014).

[23] D. Amoroso and S. Picozzi, Phys. Rev. B **93,** 214106 (2016).

[24] K. Irie, J. Phys. Soc. Jpn. **30,** 1506 (1971).

[25] B. Kundys, Appl. Phys. Rev. **2,** 011301 (2015).

[26] K. Irie, J. Phys. Soc. Jpn. **34,** 1530 (1973).

[27] D. Daranciang, M. J. Highland, H. Wen, S. M. Young, N. C. Brandt, H. Y. Hwang, M. Vattilana, M. Nicoul, F. Quirin, J. Goodfellow, T. Qi, I. Grinberg, D. M. Fritz, M. Cammarata, D. Zhu, H. T. Lemke, D. A. Walko, E. M. Dufresne, Y. Li, J. Larsson, D. A. Reis, K. Sokolowski-Tinten, K. A. Nelson, A. M. Rappe, P. H. Fuoss, G. B. Stephenson, and A. M. Lindenberg, Phys. Rev. Lett. **108,** 087601 (2012).

[28] L. Braun, G. Mussler, A. Hruban, M. Konczykowski, T. Schumann, M. Wolf, M. Münzenberg, L. Perfetti, and T. Kampfrath, Nature Commun. **7,** 13259 (2016).

[29] M. Nakamura, S. Horiuchi, F. Kagawa, N. Ogawa, T. Kurumaji, Y. Tokura, and M. Kawasaki, Nature Commun. **8,** 281 (2017).

[30] K. Irie and K. Ohi, J. Phys. Soc. Jpn. **28,** 1379 (1970).

[31] Z. Gu, D. Imbrenda, A. L. Bennett-Jackson, M. Falmbigl, A. Podpirka, T. C. Parker, D. Shreiber, M. P. Ivill, V. M. Fridkin, and J. E. Spanier, Phys. Rev. Lett. **118,** 096601 (2017).

[32] A. Kikuchi and E. Sawaguchi, J. Phys. Soc. Jpn. **25,** 1195 (1968).

FIG. 1. (a) Crystal structure of SbSI. The spontaneous polarization appears along the c-axis. (b) Temperature dependence of electric polarization measured after $\pm$208 V/cm ($\pm P$) poling. s-polarized ($//c$-axis) SHG in reflection geometry is also plotted (open-circles). (c) Photocurrent spectra at 260 K with and without bias voltage (after $+P$ poling) plotted together with the reflectivity. Incident light is not polarized and covers whole sample surface but not electrodes. Reflectivity was measured on the center of the sample with a 250 μm$\square$ aparture. bg: band gap. (d) Absolute value of the zero-bias current after $+P$ poling in the warming run. Pyroelectric current (orange curve) is not subtracted. (e,f) I-V characteristics under varying light intensity for $\pm P$ poling. For (d)-(f), a laser diode (LD) polarized along the c-axis ($E(\omega)//c$) is focused on a 100 μmϕ spot at the center of the sample.

FIG. 2. Relaxation of zero-bias photocurrent (in absolute value) with LD (a) and pulsed laser (120 fs, 1 kHz) (b) illumination at 260 K. The irradiation starts at Time = 10 minutes. Insets show the integrated charge amount. Lasers are polarized along the c-axis ($E(\omega)//c$) and focused on a 100 μmϕ spot at the center of the sample.

FIG. 3. (a) Photograph of a sample single crystal with Ag electrodes. Red closed circle indicates the illumination spot (focused to $\sim$100 μmϕ), polarized along the c-axis ($E(\omega)//c$). (b,c) Illumination position dependence of the drift (b) and zero-bias (c) photocurrent at 260 K. For (b), bias of $\pm$208 V/cm is applied. A LD light source (1.95 eV/2.4 mW) is focused on a 100 μm spot, and scanned along the c-axis. In (c), data measured with pulsed laser (1.95 eV/0.6 μJ) is also plotted with filled circles connected with solid lines. (d) Time traces of the photocurrent measured at three representative points indicated in (c) (offset for clarity). (e) Photo-Hall current measured with additional electrodes attached near the center of the sample (light blue arrows in (a)).

FIG. 4. (a) Photon energy and (b) temperature dependence of pulsed photocurrent (offset for clarity). A pulsed laser polarized along the c-axis ($E(\omega)//c$) is focused on a 100 μmϕ spot at the center of the sample. (c) Integrated photocurrent corresponding to the time-traces in (b). The presence of transient anomalies, i.e., reversed photocurrent to that from shift current, are indicated by blue shaded regions. (d) Time traces of the photocurrent under varying bias voltage after $+P$ poling (offset for clarity). Small peaks around 18 ns are due to the reflection ringing in the circuit.

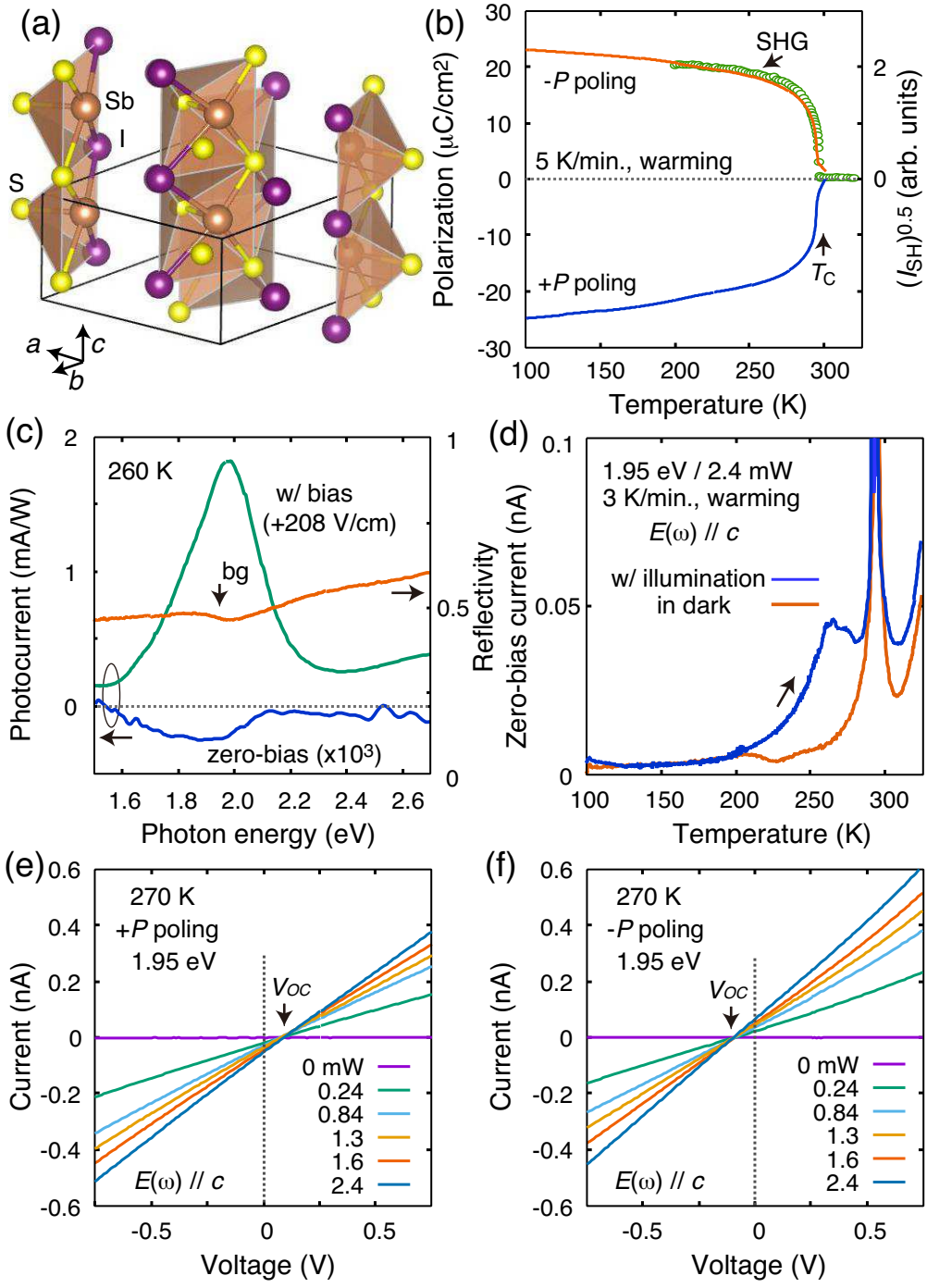

Figure 1 07Dec2017

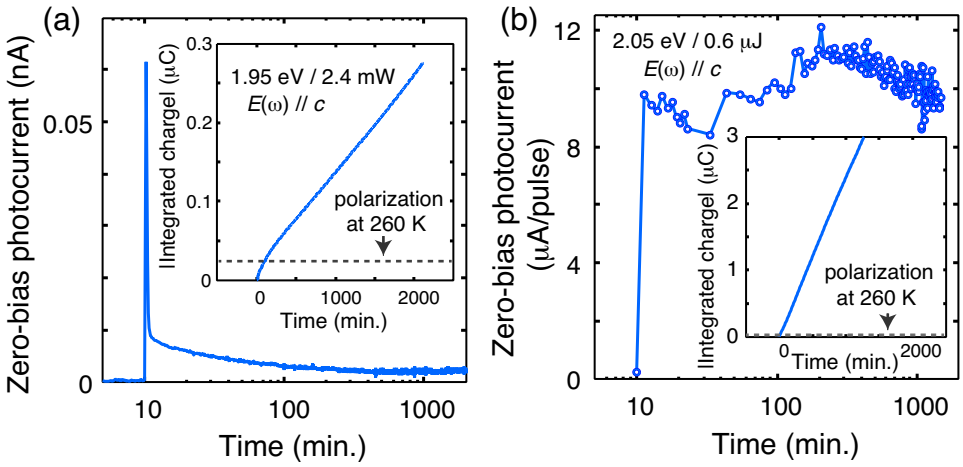

Figure 2 07Dec2017

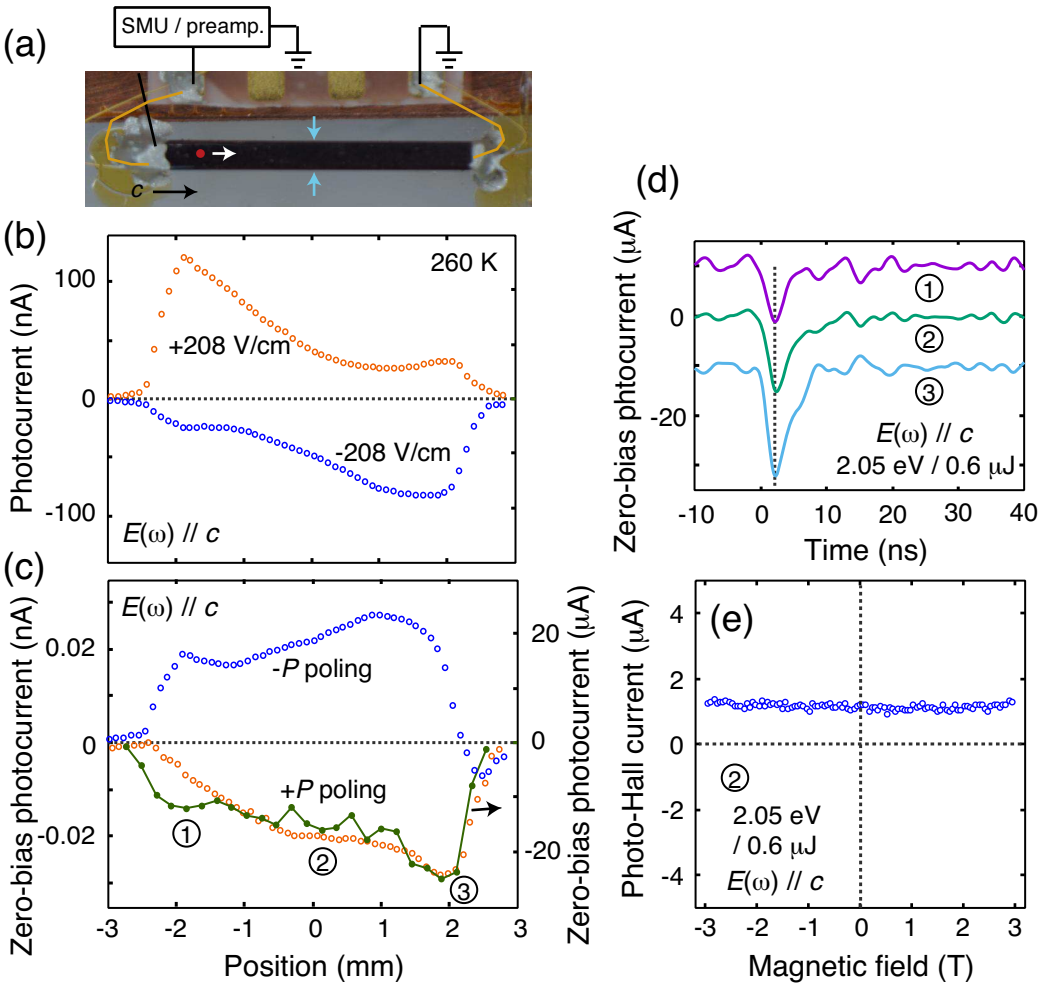

Figure 3 07Dec2017

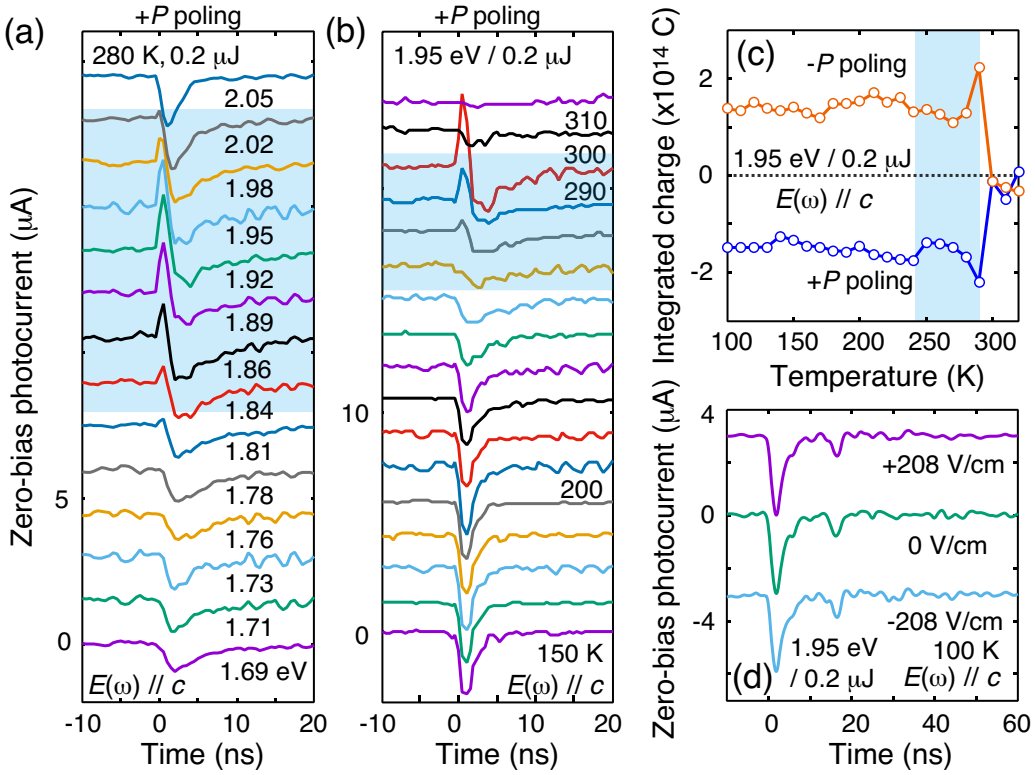

Figure 4 07Dec2017